Submitted to *INFORMS Journal on Computing*
manuscript (Please, provide the manuscript number!)

Communication-Constrained Expansion Planning for Resilient Distribution Systems

Geunyeong Byeon and Pascal Van Hentenryck
Industrial and Operations Engineering, University of Michigan

Russell Bent and Harsha Nagarajan
Los Alamos National Laboratory

Distributed generation and remotely controlled switches have emerged as important technologies to improve the resiliency of distribution grids against extreme weather-related disturbances. Therefore it becomes important to study how best to place them on the grid in order to meet a resiliency criteria, while minimizing costs and capturing their dependencies on the associated communication systems that sustain their distributed operations. This paper introduces the Optimal Resilient Design Problem for Distribution and Communication Systems (ORDPDC) to address this need. The ORDPDC is formulated as a two-stage stochastic mixed-integer program that captures the physical laws of distribution systems, the communication connectivity of the smart grid components, and a set of scenarios which specifies which components are affected by potential disasters. The paper proposes an exact branch-and-price algorithm for the ORDPDC which features a strong lower bound and a variety of acceleration schemes to address degeneracy. The ORDPDC model and branch-and-price algorithm were evaluated on a variety of test cases with varying disaster intensities and network topologies. The results demonstrate the significant impact of the network topologies on the expansion plans and costs, as well as the computational benefits of the proposed approach.

Key words: Planning for Resiliency, Power Systems, Branch and Price

1. Introduction

The last decades have highlighted the vulnerability of the current electric power system to weather-related extreme events. Between 2007 and 2016, outages caused by natural hazards, such as thunderstorms, tornadoes, and hurricanes, amounted to 90 percent of major electric disturbances, each affecting at least 50,000 customers (derived from Form OE-417 of U.S. DOE). It is also estimated that 90 percent of all outages occur along distribution systems (Executive Office of the President 2013). Moreover, the number of

weather-related outages is expected to rise as climate change increases the frequency and intensity of extreme weather events (Executive Office of the President 2013). Accordingly, it is critical to understand how to harden and modernize distribution grids to prepare for potential natural disasters.

Distributed Generation (DG) is one of the advanced technologies that can be utilized to enhance grid resilience. DG refers to electric power generation and storage performed by a collection of distributed energy resources (DER). DG decentralizes the electric power distribution by supplying power to the loads closer to where it is located. The potential of DGs is realized via a system approach that views DGs and associated loads as a microgrid (Lasseter et al. 2002). A microgrid is often defined as a small-scale power system on medium- or low- voltage distribution feeder that includes loads and DG units, together with an appropriate management and control scheme supported by a communication infrastructure (Resende et al. 2011). When faults occur in the main grid, microgrids can be detached from the main grid and act in island mode to serve critical loads by utilizing local DGs or work in the grid-connected mode to provide ancillary services for the bulk system restoration (Wang et al. 2016a). Remotely controlled switches (RCS), another advanced technology, can be used to increase the grid flexibility by controlling the grid topology through a communication network and facilitate microgrid formations in emergencies. Other than the aforementioned operational enhancement measures, a grid can also be hardened physically by installing underground cables and/or upgrading the overhead lines with stronger materials, which reduces the physical impact of catastrophic events (Panteli et al. 2017).

A critical issue in building resilient distribution grids is to determine where to place such advanced devices (i.e., DGs, RCSs, and underground cables) and which existing lines to harden. It is also important to understand the dependency between the distribution grid and its associated communication network, which is critical to the effective operation of a modernized grid during emergency situations and is also vulnerable to extreme events (Falahati et al. 2012, Gholami et al. 2016, Martins et al. 2017, Li et al. 2017).

To address this pivotal and pressing issue, this paper introduces the Optimal Resilient Design Problem for Distribution and Communication Systems (ORPDDC). The ORDPDC determines how to harden and modernize an interdependent network to ensure its resilience against extreme weather events. Like recent papers (e.g., Yamangil et al. (2015), Barnes

et al. (2017), the ORDPDC takes into account a set of disaster scenarios, each defining a set of power system components that are damaged during an extreme event. These scenarios are generated from probabilistic models of how power system components respond to hazard-specific stress (e.g., wind speed and flood depth) that are derived from historical data. The ORDPDC considers the following upgrade options: a set of hardening options on existing power lines and communication links and a set of new components that can be added to the system—new lines, new communication pathways, remotely controlled switches, and distributed generation. The objective of the ORDPDC is to find the cheapest set of upgrade options that can be placed on the grid in order to guarantee that a minimal amount of critical and non-critical load be served in each scenario. These guarantees are called the resiliency criteria.

The ORDPDC is modeled with a two-stage stochastic mixed integer program. The first stage decides an upgrade profile and the second stage decides how to utilize the DGs, RCSs, and power lines/communication links, whose availability is decided in the first-stage, to restore critical loads up to resiliency criteria (e.g., 98 %) in each disaster scenario. For each scenario, the second stage is viewed as a restoration model that identifies how to reconfigure the grid. Within this second stage problem, the physics of power flows is modeled with the steady-state, unbalanced three phase AC power equations and constraints that ensure that the radial structure of distribution grids is maintained. When the grid is reconfigured due to some disturbances, each island or microgrid must be connected to at least one control center that coordinates its DGs and loads and operates its RCSs. This communication requirement is modeled with a single-commodity flow model.

Several solution methods can be used to solve the ORDPDC, taking advantage of its block diagonal structure. Yamangil et al. (2015) proposed a Scenario-Based Decomposition (SBD) algorithm that restricts attention to a smaller set of scenarios and adds new ones on an as needed basis (see Section 5). However, in the worst case, the SBD algorithm must solve the large-scale ORDPDC as a whole. Another Scenario Decomposition (SD) algorithm was proposed by Ahmed (2013) that explores solutions to each subproblem as candidate primal feasible solutions for the overall problem (see Section 5). However, a strong performance of the SD algorithm is guaranteed only when the probability that an ϵ-optimal solution of the overall problem (for small enough $\epsilon > 0$) becomes the optimal solution to a realization is strictly positive. Hence, in the worst case, it may explore all

feasible solutions of each subproblem. Branch and Price (B&P), which combines column generation and branch-and-bound, is another solution method for approaching large-scale mixed-integer programming (Lübbecke and Desrosiers 2005). Although widely successful on many applications, it may suffer from degeneracy and long-tail effects as problems become larger. To address these difficulties, several stabilization techniques have been proposed and proven to be effective in many applications (e.g., (Du Merle et al. 1999, Oukil et al. 2007, Amor et al. 2009)). Nevertheless, the high degree of degeneracy and the significant scale of the ORDPDC create significant challenges for dual stabilization techniques.

To address these computational challenges, this paper proposes a B&P algorithm that systematically exploits the structure of the ORDPDC. The algorithm starts with a compact reformulation that results in strong lower bounds on the test cases and pricing subproblems that are naturally solved in parallel. Moreover, the B&P algorithm tackles the degeneracy inherent in the ORDPDC through a variety of acceleration schemes for the pricing subproblems: A pessimistic reduced cost, an optimality cut, and a lexicographic objective. The resulting B&P algorithm produces significant computational improvements compared to existing approaches.

The key contributions of this paper can be summarized as follows:

- The paper proposes the first planning model for resilient distribution networks that combines the use of advanced technologies (e.g., DGs, RCSs, and undergrounding) with traditional hardening options and captures the dependencies between the distribution grid and its associated communication system.
- The paper proposes an exact B&P algorithm for solving the ORDPDC, which systematically exploits the ORDPDC structure to obtain strong lower bounds and address its significant degeneracy issues.
- The paper evaluates the impact of grid and communication system topologies on potential expansion plans. It also reports extensive computational results demonstrating the benefits of the proposed B&P algorithm on the test cases.

The remainder of this paper is organized as follows. Section 2 reviews related work on the ORDPDC. Section 3 formalizes the ORDPDC and Section 4 presents a tight linear approximation. Section 5 briefly reviews the SBD and SD algorithms. Section 6 presents the new B&P algorithm. Section 7 describes the test cases. Lastly, Section 8 analyzes the behavior of the model on the case studies and Section 10 reports on the computational performance of the proposed algorithm. Section 11 concludes the paper.

2. Literature Review

There has been a considerable progress in advancing methods that address weather-related issues at distribution level (Wang et al. 2016a). Many studies develop post-fault distribution system restoration (DSR) models to bring power back as soon as possible and restore critical loads after a severe outage. Recently, DGs, RCSs, and redundant lines were utilized to leverage microgrids in load restoration. Most of the studies assume the existence of those devices beforehand (Chen et al. 2016, Ding et al. 2017, Gao et al. 2016, Yuan et al. 2017). Wang et al. (2016b) proposed a DSR model that utilizes the placement of dispatchable DGs. The above-mentioned studies however propose post-contingency models. To facilitate these novel restoration methods, the devices should be placed in suitable places in advance. This paper focuses on the optimal placement of those devices so that the grid survives potential weather-related events.

Only a limited number of studies have discussed how to optimally add resilience to distribution networks. Most relevant is the work by Barnes et al. (2017) and Yamangil et al. (2015) who propose multi-scenario models for making a distribution grid resilient with respect to a set of potential disaster scenarios. They propose decomposition-based exact and heuristic solution approaches. However, these studies do not take into account the grid's functional dependencies on the associated communication network. Accordingly, the possible faults in the communication network are not considered and the upgrade options only consider the power grid, not the communication network. Yuan et al. (2016) proposed a two-stage robust optimization model by utilizing a bi-level network interdiction model that identifies the critical components to upgrade for the resilience against the $N-K$ contingency criterion. However, as pointed out in Barnes et al. (2017), in practice, the computational complexity of this approach grows quickly with the number of allowable faults. The study also did not explicitly consider the dependency on the communication network: A DG can supply power to the node it is placed on and its children if they are not damaged by the attack. Carvalho et al. (2005) and Xu et al. (2016) discuss how to place RCSs in distribution systems, but only single fault scenarios are assumed, which is not suitable for capturing weather-related extreme events.

As the instrumentation of the grid increases, frameworks for modeling its dependence on communication networks from a resilience viewpoint have been studied (Martins et al. 2017, Parhizi et al. 2015). Resende et al. (2011) proposed a hierarchical control system,

which assumes the existence of a controller in each microgrid to allow the coordination among distributed generation units in the microgrid, while multiple microgrids are organized by a central management controller. On the other hand, distributed control systems are applied to microgrids where there are many devices with their own controllers. Accordingly, Chen et al. (2016) assumed that RCSs have local communication capabilities to exchange information with neighboring switches over short-range low-cost wireless networks and proposed a global information discovery scheme to get the input parameters for a DSR model. However, the assumption that RCSs are installed in all lines is premature for current distribution systems. Wang et al. (2016b) proposed a two-layered communication framework where the lower-layer cyber network supports microgrids where local control systems are installed, while the upper-layer network is composed of multiple local control systems that only communicate with their neighboring counterparts. The study can be viewed as a hybrid of centralized and decentralized framework: At a microgrid level, it is operated in a centralized fashion, while the upper-level network is operated in a decentralized manner. However, it did not consider fault scenarios in communication networks. This paper only assumes the lower-layer cyber network proposed in Wang et al. (2016b) by dynamically allocating a local control system to each microgrid in islanding mode. Moreover, this paper also considers potential faults in the communication system.

To the best of our knowledge, this paper proposes, for the first time, an exact optimization algorithm for expanding an integrated distribution grid and communication network through the placement of new DGs and RCSs and the hardening of existing lines in order to ensure resilience against a collection of disaster scenarios.

3. The ORDPDC

The ORDPDC considers an unbalanced three-phase distribution grid coupled with a communication network, as illustrated in Figure 1. In the figure, blue- and red-colored arrows represent regular and critical loads. Nodes in the communication networks may control a generator or a switch in the distribution network, as indicated by dotted lines. The figure also highlights how the line phases are interconnected at the buses and the communication centers that will send instructions to generators and switches remotely.

Let $G = (V, E)$ be an undirected graph that represents a distribution grid and its available upgrade options: V and E denote the set of buses and the set of distribution lines. The

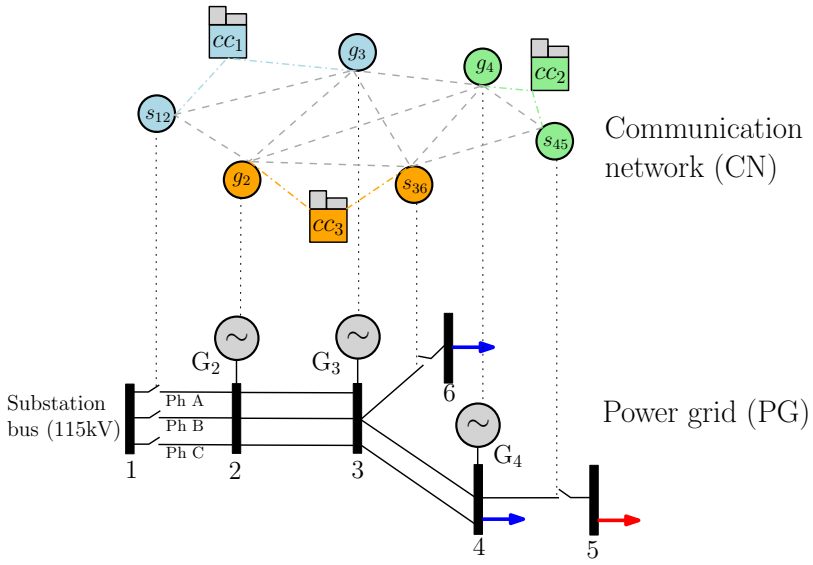

Figure 1 **The Cyber-Physical Network for Electricity Distribution. Solid lines represent power lines and dotted lines represent communication links.**

communication network, along with its potential upgrade options, is represented by a undirected graph $\widetilde{G} = (\widetilde{N}, \widetilde{E})$, where $\widetilde{N}$ and $\widetilde{E}$ are the set of communication nodes and a set of communication links. A communication node is either a control point or an intermediate point. Each control point is associated with some device in G and some nodes in $\widetilde{N}$ are designated as control centers.

The power grid G depends on its communication network $\widetilde{G}$ in the following way: A device in G (e.g., a generator or a RCSs) is operable only when its associated control point can receive a signal from some control center in $\widetilde{G}$. This modeling enables islands to form and to be operated independently only when at least one control center can communicate to the island and, in particular, its generator(s).

Let $\mathcal{G} = (\mathcal{N}, \mathcal{E})$ be the integrated system of G and $\widetilde{G}$ with $\mathcal{N} = N \cup \widetilde{N}$ and $\mathcal{E} = E \cup \widetilde{E}$. Let $\mathcal{D}$ be a set of damage scenarios for $\mathcal{G}$ indexed with $\mathcal{S} := \{1, \cdots, |\mathcal{D}|\}$. Each scenario $s \in \mathcal{S}$ is a set of edges of $\mathcal{E}$ that are damaged under s. The goal of the ORDPDC is to find an optimal upgrade profile for the cyber-physical system $\mathcal{G}$ that is resilient with respect to the damage scenarios in $\mathcal{D}$. The upgrade options include a) the building of new edges in $\mathcal{E}$ (i.e., distribution lines or communication links); b) the building of RCSs on some lines in E to provide operational flexibility; c) the hardening of existing edges in $\mathcal{E}$ to lower the probability of damage, and d) the building of DGs at some buses of the grid.

The ORDPDC is a two-stage mixed integer stochastic program. The first-stage variables represent potential infrastructure enhancements for the coupled network $\mathcal{G}$ and the second-stage variables capture how upgrades serve the loads in each disaster scenario.

3.1. Mathematical Formulation

Table 1 specifies the input data for the ORDPDC problem, while Table 2 describes the model variables. The formulation assumes that all new and hardened lines come with switches (i.e., $\mathcal{E}_x^n \cup \mathcal{E}_h \subseteq \mathcal{E}_t^0$) which reflects current industry practice. Throughout this paper, an edge $e \in \mathcal{E}$ is represented as an ordered pair (e_h, e_t) for some $e_h, e_t \in \mathcal{N}$ and $\delta(e) = \{e_h, e_t\}$. The set of all edges incident to a node $i \in \mathcal{N}$ is denoted by $\delta(i)$. The notation $x_{\mathcal{A}}$ represents the projection of a vector x to the space of some index set $\mathcal{A}$, i.e., $(x_a)_{a\in\mathcal{A}}$: For instance, $x^s_{\mathcal{E}_x} = (x^s_e)_{e\in\mathcal{E}_x}$.

The presentation uses $w = (x_{\mathcal{E}_x^n}, t_{\mathcal{E}_t^n}, h_{\mathcal{E}_h}, u_{\mathcal{U}^n})$ to denote upgrade profiles, m the dimension of w, $c = (c^x_{\mathcal{E}_x^n}, c^t_{\mathcal{E}_t^n}, c^h_{\mathcal{E}_h}, c^u_{\mathcal{U}^n}) \in \mathbb{R}^m$ the cost vector, and $w^s = (x^s_{\mathcal{E}_x^n}, t^s_{\mathcal{E}_t^n}, h^s_{\mathcal{E}_h}, u^s_{\mathcal{U}^n})$ feasible upgrade profiles for each scenario $s \in \mathcal{S}$. For each $s \in \mathcal{S}$, $\mathcal{Q}(s)$ denotes the set of upgrade profiles that enable the grid to maintain the predetermined load satisfaction (resiliency) level η_c, η_t (e.g., $\eta_c = 0.98$ and $\eta_t = 0.5$) under disaster scenario s.

With these notations, the ORDPDC is formulated as follows:

$$
\begin{aligned}
(P) \quad \min \quad & c^T w && && \text{(1a)}\\
\text{s.t.} \quad & w \geq w^s, && \forall s \in \mathcal{S}, && \text{(1b)}\\
& w^s \in \mathcal{Q}(s), && \forall s \in \mathcal{S}, && \text{(1c)}\\
& w \in \{0,1\}^m. && && \text{(1d)}
\end{aligned}
$$

Problem (P) tries to find the optimal upgrade profile $w^* = (x^*_{\mathcal{E}_x^n}, t^*_{\mathcal{E}_t^n}, h^*_{\mathcal{E}_h}, u^*_{\mathcal{U}^n})$ that ensures resilient operations for each disaster scenario. Constraint (1b) ensures that an upgrade profile is feasible if it dominates a feasible solution $w^s \in \mathcal{Q}(s)$ for each scenario s, i.e., if the grid survives each of the extreme events in $\mathcal{S}$.

The set $\mathcal{Q}(s)$ is specified by resiliency constraints that are expressed in terms of the AC power flow equations, load satisfaction requirements, the communication network, and the grid topology:

$$\mathcal{Q}(s) = \{w^s \in \{0,1\}^m : (2), (3), (4), (5), \text{ and } (6)\}$$

where Constraints (2), (3), (4), (5), and (6) are stated in detail in the following. The variables in each $\mathcal{Q}(s)$ are indexed by s. For simplicity, this section omits index s.

Table 1 The Parameters of the ORDPDC.

$G=(N,E)$	an undirected extended distribution grid with available upgrade options
$\mathcal{U}:=\mathcal{U}^0\cup\mathcal{U}^n$	a set of generators, indexed with l
$\mathcal{U}^0$	a set of existing generators
$\mathcal{U}^n$	a set of generators that can be installed
$i(l)\in N$	the bus in which the generator $l\in\mathcal{U}$ is located
$\mathcal{U}_i\subseteq\mathcal{U}$	the set of generators connected to bus $i\in N$
$E_V\subseteq E$	a set of transformers
β_e	maximum flow variation allowed between different phases on line $e\in E_V$
$\mathcal{C}\subseteq 2^{\lvert E\rvert}$	a collection of a set of edges which forms a cycle with a distinct node set
$\mathcal{P}_e,\mathcal{P}_i,\mathcal{P}_l$	a set of phases on line $e\in E$, bus $i\in N$, and generator $l\in\mathcal{U}$, respectively
T_e^k	a thermal limit on line $e\in E$ for phase $k\in\mathcal{P}_e$
$\underline{V}_i^k,\overline{V}_i^k$	lower and upper bound on voltage magnitude at bus $i\in N$ on phase $k\in\mathcal{P}_i$
$Z_e=R_e+\mathbf{i}\ X_e$	phase impedance matrix of line $e\in E$
$\mathcal{L}\subseteq N$	a set of buses with critical loads
$D_{i,p}^k+\mathbf{i}\ D_{i,q}^k$	complex power demand at bus $i\in N$ on phase $k\in\mathcal{P}_i$
η_c,η_t	resiliency criteria in percentage for critical and total loads respectively
$\overline{g}_{l,p}^k+\mathbf{i}\ \overline{g}_{l,g}^k$	complex power generation capacity of generator $l\in\mathcal{U}$ on phase $k\in\mathcal{P}_l$
$\widetilde{G}=(\widetilde{N},\widetilde{E})$	an extended associated communication network with potential upgrade options
$\widetilde{N}_c:=\widetilde{N}_t\cup\widetilde{N}_u$	
$\widetilde{N}_t\subseteq\widetilde{N}$	a set of control points for switches
$\widetilde{N}_u\subseteq\widetilde{N}$	a set of control points for generators
$\tilde{i}(e)\in\widetilde{N}_t,\tilde{i}(l)\in\widetilde{N}_u$	the control point in $\widetilde{G}$ of a switch $e\in\mathcal{E}_t$ and a generator $l\in\mathcal{U}$, respectively
$\tilde{i}_d\in\widetilde{N}$	an artificial dummy node in $\widetilde{G}$
$\mathcal{G}=(\mathcal{N},\mathcal{E})$	the integrated system of G and $\widetilde{G}$
$\mathcal{E}_x:=\mathcal{E}_x^0\cup\mathcal{E}_x^n$	
$\mathcal{E}_x^0\subseteq\mathcal{E}$	a set of existing lines and links
$\mathcal{E}_x^n\subseteq\mathcal{E}$	a set of lines and links that can be installed
$\mathcal{E}_t:=\mathcal{E}_t^0\cup\mathcal{E}_t^n$	
$\mathcal{E}_t^0\subseteq E$	a set of lines in which a switch is installed
$\mathcal{E}_t^n\subseteq E$	a set of lines in which a switch can be installed
$\mathcal{E}_h\subseteq E$	a set of lines or links that can be hardened
c_e^x	installation cost of $e\in\mathcal{E}_x^n$
c_e^t	installation cost of switch on $e\in\mathcal{E}_t^n$
c_e^h	line hardening cost of $e\in\mathcal{E}_h$
c_l^u	installation cost of $l\in\mathcal{U}^n$ on the corresponding bus
$\mathcal{D}$	a collection of sets of damaged lines for each scenario, indexed with $\mathcal{S}:=\{1,\cdots,\lvert\mathcal{D}\rvert\}$

3.1.1. Power Flow Constraints Figure 2 specifies the power flow equations and summarizes some of the notations. Let $\mathcal{P}=\{a,b,c\}$ denote the three phases of the network. For each bus $i\in N$, define $V_i=(V_i^k)_{k\in\mathcal{P}_i}$ and, for each line $e\in E$, define $I_e=(I_e^k)_{k\in\mathcal{P}_e}$ and $s_{e,i}=(s_{e,i}^k)_{k\in\mathcal{P}_e}$. The notations also use a superscript $\mathcal{P}'\subseteq\mathcal{P}$ to represent the *projection* or the *extension* of a vector to the space of $\mathcal{P}'$. For example, if $\mathcal{P}_i=\{a,b,c\}$ and $\mathcal{P}'=\{a,b\}$, then $V_i^{\mathcal{P}'}=\left(V_i^a,V_i^b\right)^T$. If $\mathcal{P}_i=\{a,c\}$ and $\mathcal{P}'=\{a,b,c\}$, then $V_i^{\mathcal{P}'}=\left(V_i^a,0,V_i^c\right)^T$.

For each line $e=(i,j)\in E$, Ohm's law for 3-phase lines states the relationship $V_j^{\mathcal{P}_e}=V_i^{\mathcal{P}_e}-Z_eI_e$ between I_e, V_i, and V_j. For each line $e\in E$ and bus $i\in\delta(e)$, the electric power

Table 2 The Variables of the ORDPDC.

Binary variables	
x_e	1 if $e \in \mathcal{E}_x^n$ is built
t_e	1 if a switch is built on $e \in \mathcal{E}_t^n$
h_e	1 if $e \in \mathcal{E}_h$ is hardened
u_l	1 if a generator $l \in \mathcal{U}^n$ is built.
For each disaster scenario $s \in \mathcal{S}$,	
z_e^s	1 if $e \in \mathcal{E}$ is active during s
x_e^s	1 if $e \in \mathcal{E}_x$ exists during s
t_e^s	1 if a switch on e is used or not during s
h_e^s	1 if $e \in \mathcal{E}_h$ is hardened during s
u_l^s	1 if a generator $l \in \mathcal{U}^n$ is available during s
y_e^s	1 if $i,\ j \in N$ can be disconnected, for $e = (i,j) \in C,\ C \in \mathcal{C}$, during s
b_e	1 if the real power on line $e = (i,j) \in E$ flows from j to i during s
b'_e	1 if the reactive power on line $e = (i,j) \in E$ flows from j to i during s
Continuous variables	
For each disaster scenario $s \in \mathcal{S}$,	
$d_i^{s,k} = d_{i,p}^{s,k} + \mathbf{i}\ d_{i,q}^{s,k}$	amount of power delivered at bus $i \in N$ on phase $k \in \mathcal{P}_i$ during s
$g_l^{s,k} = g_{l,p}^{s,k} + \mathbf{i}\ g_{l,q}^{s,k}$	amount of power generation of $l \in \mathcal{U}$ on phase $k \in \mathcal{P}_l$ during s
$s_{e,i}^{s,k} = p_{e,i}^{s,k} + \mathbf{i}\ q_{e,i}^{s,k}$	power flow on i-end of line $e \in E$, where $i \in \delta(e)$, on phase $k \in \mathcal{P}_e$ during s
$V_i^{s,k}$	complex voltage at bus $i \in N$ on phase $k \in \mathcal{P}_i$ during s
$I_e^{s,k}$	complex current on line $e \in E$ on phase $k \in \mathcal{P}_e$ during s
$v_i^{s,k}$	squared voltage magnitude at bus $i \in N$ on phase $k \in \mathcal{P}_i$ during s
f_e^s	the amount of artificial flow on $e \in \widetilde{E}$ during s
$\gamma_{\tilde{i}}^s$	indicator of connectivity of control point $\tilde{i} \in \widetilde{N}$ to some control center during s

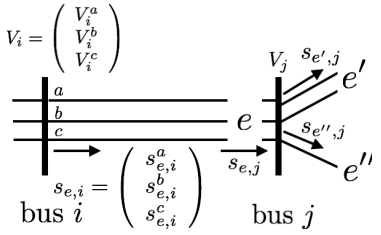

$$-M(1-z_e) \le V_j^{\mathcal{P}_e} - (V_i^{\mathcal{P}_e} - Z_e I_e) \le M(1-z_e), \qquad \forall e=(i,j)\in E, \quad (2a)$$

$$s_{e,i} = \mathrm{diag}(V_i^{\mathcal{P}_e} I_e^H), \qquad \forall e \in E, i \in \delta(e), \quad (2b)$$

$$\sum_{l\in\mathcal{U}_i} g_l^k - d_i^k = \sum_{e\in\delta(i)} s_{e,i}^k, \qquad \forall i \in N, k \in \mathcal{P}_i \quad (2c)$$

$$(p_{e,i}^k)^2 + (q_{e,i}^k)^2 \le (T_e^k)^2 z_e, \qquad \forall e \in E, i \in \delta(e), k \in \mathcal{P}_e, \quad (2d)$$

$$\underline{V}_i^k \le |V_i^k| \le \overline{V}_i^k, \qquad \forall i \in N, k \in \mathcal{P}_i. \quad (2e)$$

$$-b_e T_e^k \le p_{e,i}^k \le T_e^k (1-b_e), \qquad \forall e=(i,j)\in E, k \in \mathcal{P}_e, \quad (2f)$$

$$-b'_e T_e^k \le q_{e,i}^k \le T_e^k (1-b'_e), \qquad \forall e=(i,j)\in E, k \in \mathcal{P}_e, \quad (2g)$$

Figure 2 Notations for the Power Flow Equations.

flow equation $s_{e,i} = \mathrm{diag}(V_i^{\mathcal{P}_e} I_e^H)$ describes the relationship between $s_{e,i}$, $V_i^{\mathcal{P}_e}$, and I_e, where superscript H indicates the conjugate transpose. In Figure 2, the big-M method is used in Constraint (2a) to apply Ohm's law only for available lines; the big-M can be set as $\max_{j'\in\{i,j\},k\in\mathcal{P}_e} \overline{V}_{j'}^k - \min_{j'\in\{i,j\},k\in\mathcal{P}_e} \underline{V}_{j'}^k$. Equation (2c) is the balance equation for power flow at each bus $i \in N$, i.e., the sum of incoming flows equals the sum of the outgoing flows.

Let $p_{e,i} + \mathbf{i}q_{e,i}$ be the rectangular representation of $s_{e,i}$, where $p_{e,i} = (p^k_{e,i})_{k\in\mathcal{P}_i}$ and $q_{e,i} = (q^k_{e,i})_{k\in\mathcal{P}_i}$ denote the real and reactive power at the i-end of line e. Constraints (2d) and (2e) specify the thermal limits on lines and the voltage bounds on buses.

In some disaster scenarios when some of the lines are broken, power flows of different phases on the same line can have opposite directions, which is very undesirable operationally. Constraints (2f) and (2g) prevent this behavior from happening.

The real and reactive power on different phase must stay within a certain limit. Let $\widehat{p}_{e,i} = \sum_{\tilde{k}\in\mathcal{P}_e} p^{\tilde{k}}_{e,i}$ and $\widehat{q}_{e,i} = \sum_{\tilde{k}\in\mathcal{P}_e} q^{\tilde{k}}_{e,i}$. Then, these limits are formulated as follows:

$$\left(\underline{\beta}_e(1-b_e) + \overline{\beta}_e b_e\right)\frac{\widehat{p}_{e,i}}{|\mathcal{P}_e|} \le p^k_{e,i} \le \left(\underline{\beta}_e b_e + \overline{\beta}_e(1-b_e)\right)\frac{\widehat{p}_{e,i}}{|\mathcal{P}_e|},\ \forall e\in E_V, k\in\mathcal{P}_e, \tag{3a}$$

$$\left(\underline{\beta}_e(1-b'_e) + \overline{\beta}_e b'_e\right)\frac{\widehat{q}_{e,i}}{|\mathcal{P}_e|} \le q^k_{e,i} \le \left(\underline{\beta}_e b'_e + \overline{\beta}_e(1-b'_e)\right)\frac{\widehat{q}_{e,i}}{|\mathcal{P}_e|},\ \forall e\in E_V, k\in\mathcal{P}_e, \tag{3b}$$

where $\underline{\beta}_e = 1-\beta_e$ and $\overline{\beta}_e = 1+\beta_2$.

3.1.2. Generator/resiliency Constraints Moreover, each generator $l\in\mathcal{U}$ has its own capacity and at least some percentage of critical and total loads must be satisfied as specified by the resiliency criteria η_c and η_t.

$$0 \le g^k_{l,p} \le \overline{g}^k_{l,p}u_l,\ g^k_{l,q} \le \overline{g}^k_{l,q}u_l, \qquad \forall l\in\mathcal{U}, k\in\mathcal{P}_l, \tag{4a}$$

$$0 \le d^k_{i,p} \le D^k_{i,p},\ 0 \le d^k_{i,q} \le D^k_{i,q}, \qquad \forall i\in N, k\in\mathcal{P}_i \tag{4b}$$

$$\sum_{i\in\mathcal{L}} d^k_{i,p} \ge \eta_c \sum_{i\in\mathcal{L}} D^k_{i,p}, \quad \sum_{i\in\mathcal{L}} d^k_{i,q} \ge \eta_c \sum_{i\in\mathcal{L}} D^k_{i,q}, \qquad \forall k\in\mathcal{P}, \tag{4c}$$

$$\sum_{i\in N} d^k_{i,p} \ge \eta_t \sum_{i\in N} D^k_{i,p}, \quad \sum_{i\in N} d^k_{i,q} \ge \eta_t \sum_{i\in N} D^k_{i,q}, \qquad \forall k\in\mathcal{P}. \tag{4d}$$

Constraint (4a) captures the power generation capacity constraints. Constraint (4b) states that the delivered power at each bus i should not exceed the load. Constraints (4c)-(4d) enforce the resiliency constraints.

3.1.3. Communication Constraints The operation of generators and RCSs depend on the communication network: A generator $l\in\mathcal{U}$ and a RCS on line $e\in\mathcal{E}_t$ is operable only if their associated control points $\tilde{i}(l)\in\widetilde{N}$ and $\tilde{i}(e)\in\widetilde{N}$ can receive a control signal from some control centers through $\widetilde{G}$. To capture the connectivity of a vertex to some control centers, the formulation uses a single-commodity flow model summarized in Constraints (5) in Figure 3. The formulation uses a dummy node $\tilde{i}_d$ to $\widetilde{N}$ and connect $\tilde{i}_d$ to all control centers

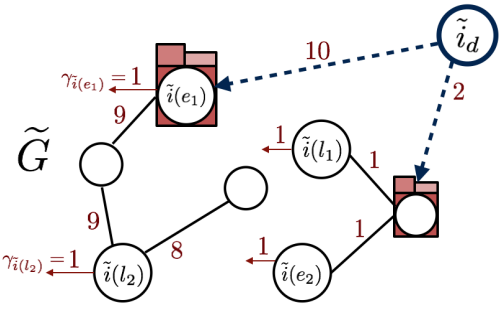

$$\sum_{e:e_t=i} f_e - \sum_{e:e_h=i} f_e = \gamma_i, \qquad \forall i \in \widetilde{N}_c, \quad (5a)$$

$$\sum_{e:e_t=i} f_e - \sum_{e:e_h=i} f_e = 0, \qquad \forall i \in \widetilde{N} \setminus (\widetilde{N}_c \cup \{\tilde{i}_d\}), \quad (5b)$$

$$-Mx_e \le f_e \le Mx_e, \qquad \forall e \in \widetilde{E}, \quad (5c)$$

$$0 \le g_l^k \le \overline{g}_l^k \gamma_{\tilde{i}(l)}, \; g_l^k \le \overline{g}_l^k \gamma_{\tilde{i}(l)}, \qquad \forall l \in \mathcal{U}, \forall k \in \mathcal{P}_l, \quad (5d)$$

$$t_e \le \gamma_{\tilde{i}(e)}, \qquad \forall e \in \mathcal{E}_t, \quad (5e)$$

$$0 \le \gamma_i \le 1, \qquad \forall i \in \widetilde{N}_c. \quad (5f)$$

Figure 3 **The Single-Commodity Flow Model for $\widetilde{G}$ (red-colored squares denote control centers).**

with additional links. The flow $f \in \mathbb{R}^{|\widetilde{E}|}$ originating from the dummy node $\tilde{i}_d$ then is used to check the connectivity of every node. By Constraint (5c), the flow passes only through available links during disaster s (the big-M value is set to $|\widetilde{N}_c|$ in the implementation). If a control point $i \in \widetilde{N}_c$ is connected with some control center through some path, it can borrow a unit of flow from f to make γ_i 1, as specified in Equations (5a) and (5b). In other words, γ_i indicates whether control point $i \in \widetilde{N}_c$ can receive a control signal. If γ_i is 1, the associated device in G is operable by Constraints (5d) and (5e).

Some communication network may be affected by a failure in distribution grid, e.g., when the grid fails to supply power to communication centers. This kind of dependencies is not considered in this paper but it can be easily captured if needed. Indeed, first assign a small critical load to each communication center and add constraints that restrict the auxiliary arcs between the dummy node and each communication center to have positive flow only when the associated communication center has a positive power supply. The constraints can be expressed in terms of an extra binary variable for each bus at which a communication center is located. The extra binary variable determines if there is a positive power supply to the communication center.

3.1.4. Topological constraints. The final set of constraints captures the topology restrictions in distribution systems:

$$x_e \ge t_e, \qquad \forall e \in \mathcal{E}, \quad (6a)$$

$$z_e = x_e - t_e, \qquad \forall e \in \mathcal{E}, \quad (6b)$$

$$x_e = h_e, \qquad \forall e \in \mathcal{D}_s, \quad (6c)$$

$$\sum_{e \in C} y_e \leq |C| - 1, \qquad \forall C \in \mathcal{C}, \tag{6d}$$

$$z_{\hat{e}} \leq y_e, \qquad \forall \hat{e} \in E : \delta(\hat{e}) = \delta(e),\ e \in C,\ C \in \mathcal{C}. \tag{6e}$$

Constraint (6a) restrict switches to be operable only on existing lines. In Equation (6b), z_e represents whether line $e \in \mathcal{E}$ is active under scenario s. A line is active when it exists and its switch is off. Equation (6c) states that a damaged line during scenario $s \in \mathcal{S}$ is inoperable unless it is hardened. Constraints (6d) and (6e) ensures that the distribution grid should operate in a radial manner. Accordingly, Constraint (6d) eliminates the sub-tours within $\mathcal{C}$. Since G is usually sparse, the implementation enumerates all the sub-tours $\mathcal{C}$ and variable y_e indicates whether $i, j \in \delta(e)$ are disconnected. If they are disconnected, then all the lines between i and j are inactive by Constraint (6e).

Note also that, for existing lines not damaged under scenario s, x_e is fixed as one. For each line $e \in E \setminus \mathcal{E}_t$, t_e is set to zero. Second, for each line $e \in \mathcal{E} \setminus \mathcal{E}_h$, h_e is fixed as 0 and all the existing generators have $u_l = 1$. Finally, for each line $e = (i, j) \in E$ with strictly decreasing or increasing phases (i.e., $|\mathcal{P}_i| > |\mathcal{P}_j|$ or $|\mathcal{P}_i| < |\mathcal{P}_j|$), the direction of power flow must be from a bus with more phases. Let $E_>$ and $E_<$ denote the set of lines with strictly decreasing and increasing phases, respectively. We add bound constraints $p^k_{e,i} \geq 0$ for $e \in E_>,\ k \in \mathcal{P}_e$ and $p^k_{e,i} \leq 0$ for $e \in E_<,\ k \in \mathcal{P}_e$. This paper assumes perfect hardening, i.e., a hardened line survives all disaster scenarios. This assumption can be naturally generalized to imperfect hardening (Yamangil et al. 2015).

4. Linearization of the ORDPDC

The formulation of the ORDPDC is nonlinear. This section discusses how to obtain a sufficiently accurate linearization.

4.1. Linear Approximation of the AC Power Flow Equations for Radial Networks

The main difficulty lies in linearizing constraints (2a–2b) for which the formulation uses the tight linearization from Gan and Low (2014). The linearization is based on two assumptions: (A1) line losses are small, i.e., $Z_e I_e I_e^H \approx 0$ for $e = (i, j) \in E$ and (A2) voltages are nearly balanced, i.e., if $\mathcal{P}_i = \{a, b, c\}$, then $V_i^a / V_i^b \approx V_i^b / V_i^c \approx V_i^c / V_i^a \approx e^{i2\pi/3}$. Informally speaking, the approximation generalizes the distflow equations to 3 phases, drops the quadratic terms, and eliminates the current variables using the balance assumption. The

derivation assumes that all phases are well-defined for simplicity. Moreover, if A is an $n \times n$ matrix, then $\text{diag}(A)$ denotes the n-dimensional vector that represents its diagonal entries. If a is an n-dimensional vector, then $\text{diag}(a)$ denotes the $n \times n$ matrix with a in its diagonal entries and zero for the off-diagonal entries.

Let $s_i = \sum_{l \in \mathcal{U}_i} g_l - d_i$ denote the power injection at bus i. By (A1), $s_{e,i} = s_{e,j}$ for all $e \in (i,j) \in E$ and therefore, given s_i, $s_{e,i}$ $(i \in \delta(e))$ is uniquely determined by Equation (2c).

Now define $S_{e,i} := V_i I_e^H$, whose diagonal entries are $s_{e,i}$. Multipling both sides of $V_j = V_i - Z_e I_e$ with their conjugate transposes gives

$$V_j V_j^H = V_i V_i^H - S_{e,i} Z_e^H - Z_e S_{e,i}^H + Z_e I_e I_e^H Z_e^H. \tag{7}$$

By assumption (A1), this becomes

$$V_j V_j^H = V_i V_i^H - S_{e,i} Z_e^H - Z_e S_{e,i}^H \tag{8}$$

and, by restricting attention to diagonal elements only,

$$v_j = v_i - \text{diag}(S_{e,i} Z_e^H - Z_e S_{e,i}^H). \tag{9}$$

where $(v_i^k)_{k \in \mathcal{P}_i} = \text{diag}(V_i V_i^H)$ represents the squared voltage magnitude at bus $i \in N$.

By (A2), we have $S_{e,i} \approx \gamma^{\mathcal{P}_e} \text{diag}(s_{e,i})$, where

$$\gamma = \begin{bmatrix} 1 & \alpha^2 & \alpha \\ \alpha & 1 & \alpha^2 \\ \alpha^2 & \alpha & 1 \end{bmatrix} \text{ and } \alpha = e^{-i2\pi/3}.$$

As a result, Equation (9) can now be simplified as follows: for each line $e = (i,j) \in E$ and $k \in \mathcal{P}_e$,

$$v_i^k = v_j^k - \sum_{k' \in \mathcal{P}_e} 2 \left[(\alpha^{n_k - n_{k'}} R_e)^{kk'} p_{e,i}^{k'} + (\alpha^{n_k - n_{k'}} X_e)^{kk'} q_{e,i}^{k'} \right], \tag{10}$$

where $n_a = 2, n_b = 1, n_c = 0$, $R_e + \mathbf{i} X_e = Z_e$, and superscript kk' of a matrix denotes its (k,k')-entry.

In summary, Ohm's law and the power flow equation in Constraints (2a) and (2b) are approximated by Eq. (10) for all $e = (i,j) \in E$ and $k \in \mathcal{P}_e$ and the big-M is set to $\max_{j'=i,j} (\overline{V}_{j',k})^2 - \min_{j'=i,j} (\underline{V}_{j',k})^2$, along with Equation (2c). Accordingly, Constraint (2e) is replaced by the following constraint:

$$(\underline{V}_i^k)^2 \le v_i^k \le (\overline{V}_i^k)^2, \quad \forall i \in N, k \in \mathcal{P}_i.$$

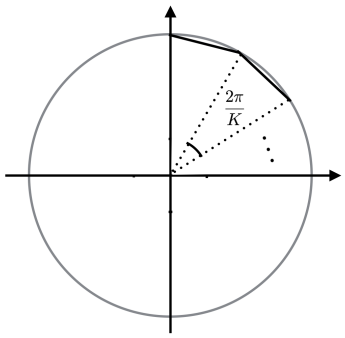

Figure 4 The Piecewise-Linear Inner Approximation of a Circle.

4.2. Linearization of (3a)-(3b)

Constraints (3a) and (3b) contain products of a binary variable and a bounded real variable. These constraints are linearized without loss of accuracy using McCormick inequalities McCormick (1976).

4.3. Piecewise-Linear Inner Approximation of Thermal Limits

The quadratic thermal limit constraint (Constraint (2d)) can be approximated with K linear inequalities as shown in Figure 4. The resulting inequalities are as follows: for all $e \in E$, $i \in \delta(e)$, $k \in \mathcal{P}_e$:

$$\left(\sin\left(\frac{2n\pi}{K}\right) - \sin\left(\frac{2(n-1)\pi}{K}\right)\right) p^k_{e,i}$$
$$- \left(\cos\left(\frac{2n\pi}{K}\right) - \cos\left(\frac{2(n-1)\pi}{K}\right)\right) q^k_{e,i} \leq \sin\left(\frac{2\pi}{K}\right) T_{e,k}, \quad \forall n = 1, \cdots, K, \tag{11a}$$
$$-M z^s_e \leq p^k_{e,i} \leq M z^s_e, \quad -M z^s_e \leq q^k_{e,i} \leq M z^s_e, \qquad \forall e \in E, k \in \mathcal{P}_e. \tag{11b}$$

where the big-M is set to $\sum_{i \in N} D^p_{i,k}$. Our implementation uses $K = 28$.

5. Scenario-Based and Scenario Decomposition

In Section 10, the branch and price algorithm presented in the next section is compared to the Scenario-Based Decomposition (SBD) and the Scenario Decomposition (SD) algorithms proposed by Yamangil et al. (2015) and Ahmed (2013) respectively.

The SBD algorithm iteratively solves a master problem $P(\mathcal{S}')$ which only includes the constraints of a subset of scenarios $\mathcal{S}' \subseteq \mathcal{S}$. The algorithm terminates when the optimal solution to $P(\mathcal{S}')$ is feasible (and hence optimal) for the remaining scenarios $\mathcal{S} \setminus \mathcal{S}'$. Otherwise, at least one scenario $s \in \mathcal{S} \setminus \mathcal{S}'$ is infeasible. Scenario s is added to $\mathcal{S}'$ and the process is repeated.

To apply the SD algorithm, consider the following equivalent problem:

$$(P') \quad \min \quad \sum_{s\in\mathcal{S}} \frac{1}{|\mathcal{S}|} c^T w^s \tag{12a}$$

$$\text{s.t.} \quad w^1 = \cdots = w^{|\mathcal{S}|}, \tag{12b}$$

$$(1c),\ (1d).$$

The equivalence follows from the assumption that all new and hardened lines come with switches (i.e., a solution that dominates a feasible solution to a subproblem can be made feasible for the subproblem by switching). Let $\sum_{s\in\mathcal{S}} A_s w^s = 0$ represent Equation (12b).

The SD algorithm explores solutions to each subproblem $P'(s),\ \forall s \in \mathcal{S}$, by minimizing the objective function $\frac{1}{|\mathcal{S}|} c^T w^s + \lambda^T A_s w^s$ to find primal feasible solutions to Problem (P'), where λ is the dual vector of Equation (12b). The explored solutions are then cut off in all subproblems to leave them out of future consideration and improve the lower bound. The algorithm proceeds until it closes the gap between lower and upper bounds.

6. The Branch-and-Price Algorithm

This paper proposes a branch-and-price (B&P) algorithm for the ORDPDC. The B&P exploits the special structure of the ORDPDC in several ways. First, it uses a compact reformulation that yields a better lower bound than the LP relaxation. The reformulation also makes it possible to use column generation and solve independent pricing problems associated with each scenario in parallel. Finally, several additional techniques are used to accelarate the column generation significantly. Section 6.1 presents the problem reformulation and Section 6.2 briefly reviews the basic column generation of the B&P algorithm. Section 6.3 introduces several acceleration schemes. The implementation of the B&P algorithm is presented in Section 6.4.

6.1. The Problem Reformulation

Letting $\widetilde{\mathcal{Q}}(s)$ be the linearization of $\mathcal{Q}(s)$, the problem (P) is rewritten as

$$(P) \quad \min \quad c^T w$$

$$\text{s.t.} \quad w - w^s \geq 0,\ \forall s \in \mathcal{S}, \tag{13a}$$

$$w^s \in \widetilde{\mathcal{Q}}(s),\ \forall s \in \mathcal{S}, \tag{13b}$$

$$w^s \in \{0,1\}^m,\ \forall s \in \mathcal{S}. \tag{13c}$$

Without the linking constraint (13a), (P) can be decomposed into $|\mathcal{S}|$ independent problems, each of which has a feasible region defined by

$$\mathcal{P}^s = \{w^s \in \mathbb{R}^m : \text{(13b) and (13c)}\}, \ \forall s \in \mathcal{S}.$$

Observe that $\mathcal{P}^s$ is bounded and let $\mathcal{J}^s = \{\hat{w}_j^s \in \mathbb{R}^m : \hat{w}_j^s \text{ is a vertex of } \text{conv}(\mathcal{P}^s)\}$ be the set of all vertices of $\text{conv}(\mathcal{P}^s)$. Letting $\mathcal{J} = \cup_s \mathcal{J}_s$, consider the following problem:

$$\begin{aligned}
(\widetilde{P}) \quad \min \quad & c^T w & & \\
\text{s.t.} \quad & w - \sum_{j \in \mathcal{J}^s} \lambda_j^s \hat{w}_j^s \geq 0, & \forall s \in \mathcal{S}, & \quad (14a)\\
& \sum_{j \in \mathcal{J}^s} \lambda_j^s = 1, & \forall s \in \mathcal{S}, & \quad (14b)\\
& w \in \{0,1\}^m, & & \quad (14c)\\
& \lambda_j^s \geq 0, & \forall j \in \mathcal{J}^s, s \in \mathcal{S}. & \quad (14d)
\end{aligned}$$

THEOREM 1. *(P) and $(\widetilde{P})$ are equivalent.*

Proof. Since (P) and $(\widetilde{P})$ have the same objective function, it suffices to show that (P) has an optimal solution that is feasible to $(\widetilde{P})$ and vice versa. Let $(\bar{w}, \{\bar{w}^s\}_{s \in \mathcal{S}})$ be the optimal solution of (P). By the Farkas-Minkowski-Weyl theorem (Schrijver 1998), for each $s \in \mathcal{S}$, $\bar{w}^s$ can be expressed as a convex combination of extreme points in $\mathcal{J}^s$, i.e., $\exists \{\bar{\lambda}_j^s\}_{j \in \mathcal{J}^s}$: $\bar{w}^s = \sum_{j \in \mathcal{J}^s} \bar{\lambda}_j^s \hat{w}_j^s, \sum_{j \in \mathcal{J}^s} \bar{\lambda}_j^s = 1$. Hence, $(\bar{w}, \{\bar{\lambda}_j^s\}_{j \in \mathcal{J}^s} \text{ for } s \in \mathcal{S})$ is feasible to $(\widetilde{P})$.

Now let $(\tilde{w}, \{\tilde{\lambda}_j^s\}_{j \in \mathcal{J}^s} \text{ for } s \in \mathcal{S})$ be an optimal solution to $(\widetilde{P})$ and note that, by (14a), if $\tilde{\lambda}_j^s > 0$ then $\hat{w}_j^s$ is dominated by $\tilde{w}$. Therefore, we can construct another optimal solution to $(\widetilde{P})$ by choosing a single j^* for which $\tilde{\lambda}_{j^*}^s > 0$ for each $s \in \mathcal{S}$ and setting $\tilde{\lambda}_{j^*}^s$ to one and the other $\tilde{\lambda}_j^s$'s to zero. Define $\tilde{w}^s = \hat{w}_{j^*}^s$ for $s \in \mathcal{S}$, then $(\tilde{w}, \{\tilde{w}^s\}_{s \in \mathcal{S}})$ is feasible to (P). □

This paper uses a branch-and-price algorithm to solve $(\widetilde{P})$. Let $LP_{\widetilde{P}}$ denote the LP relaxation of $(\widetilde{P})$. Since the feasible region of $(\widetilde{P})$ is the intersection of the convex hulls of each subproblem, $LP_{\widetilde{P}}$ yields a stronger lower bound than the LP relaxation of (P).

6.2. The Basic Branch and Price

The B&P algorithm uses a restricted master problem (M) with a subset of columns of $(\widetilde{P})$ and $|\mathcal{S}|$ independent subproblems (P_s) for $s \in \mathcal{S}$, instead of handling $LP_{\widetilde{P}}$ globally. The

column generation starts with an initial basis that consists of the first-stage variables w, a column associated with a feasible solution for each subproblem, and some slack variables. Let $\widetilde{\mathcal{J}}^s$ be the corresponding subset of $\mathcal{J}^s$. The restricted mater problem (M) is as follows:

$$
\begin{aligned}
(M) \quad & \min\ c^T w \\
& \text{s.t.} \quad w - \sum_{j \in \widetilde{\mathcal{J}}^s} \lambda_j^s \hat{w}_j^s \geq 0, && \forall s \in \mathcal{S}, && \text{(15a)} \\
& \sum_{j \in \widetilde{\mathcal{J}}^s} \lambda_j^s = 1, && \forall s \in \mathcal{S}, && \text{(15b)} \\
& w \geq 0, && && \text{(15c)} \\
& \lambda_j^s \geq 0, && \forall j \in \widetilde{\mathcal{J}}^s,\ \forall s \in \mathcal{S}. && \text{(15d)}
\end{aligned}
$$

and the pricing problem for scenario s is specified as follows:

$$
\begin{aligned}
(P_s) \quad \min \quad & -\bar{\sigma}^s + \bar{y}^{sT} w^s \\
\text{s.t.} \quad & w^s \in \widetilde{\mathcal{Q}}(s), \\
& w^s \in \{0,1\}^m,
\end{aligned}
$$

where, for scenario s, $\bar{y}^s$ is the dual solution for constraints (15a) and $\bar{\sigma}^s$ is the dual solution of the convexity constraint (15b).

6.3. Acceleration Schemes

The performance of column generation deteriorates when the master problem exhibits degeneracy, leading to multiple dual solutions which may significantly influence the quality of columns generated by the pricing problem. The master problem (M) suffers from degeneracy, especially early in the column-generation process. Initially, (M) has $(m+1)|\mathcal{S}|$ constraints, m columns corresponding to the first-stage variables w, and $|\mathcal{S}|$ columns for the second-stage variables $\{\lambda^s\}_{s\in\mathcal{S}}$. Therefore, in early iterations, linear solvers have a natural tendency to select $m(|\mathcal{S}|-1)$ columns from the slack variables in Constraints (15a). For example, assume that the slack variable is in basis for the constraint involving a non-basic first-stage variable w_k and a scenario s in Constraints (15a). By complementary slackness, this implies that the dual variable is zero. Consider a vertex $\hat{w}^s$ whose k-th entry is non-zero. The value $\bar{y}_k^s w_k^s$ is zero in the pricing problem. However, for this vertex to enter the basis, it must incur the cost c_k of w_k, which is ignored in the pricing subproblem. As a result, subproblem (P_s) prices many columns too optimistically and generates columns that do not improve the current objective value, resulting in a large number of iterations.

6.3.1. Pessimistic Reduced Cost In order to overcome the poor pricing of columns, this section first proposes a pessimistic pricing scheme that selects more meaningful columns in early iterations. Consider a solution w^s to the pricing problem. If $w^s_k = 1$ but the first-stage variable w_k is not in basis, then by the relevant constraint from (15a), the variable λ^s_j corresponding to w^s can only enter in the basis at 1 if w_k is also in the basis at 1. As a result, the pessimistic pricing scheme adds the reduced cost $c_k - \sum_{s\in\mathcal{S}} \bar{y}^s_k$ to the pricing objective, which becomes

$$-\bar{\sigma}^s + (\bar{y}^s)^T w^s + \sum_{k\in\eta}(c_k - \sum_{s\in\mathcal{S}} \bar{y}^s_k) w^s_k$$

where η is the set of indices for non-basic first-stage variables, i.e., $\eta = \{k \mid w_k \text{ is non-basic}\}$. Note that column generation with this pessimistic pricing subproblem is not guaranteed to converge to the optimal linear relaxation. Hence, the implementation switches to the standard pricing problem in later iterations.

6.3.2. Optimality Cut A solution to the master problem (M) where the first-stage variables take integer value gives an upper bound to the optimal solution. The B&P algorithm periodically solves the integer version of (M) to obtain its objective value $\bar{v}(M)$. The constraint

$$c^T w^s \leq \bar{v}(M)$$

can then be added to the pricing subproblem for scenario s since any solution violating this constraint is necessarily suboptimal. As shown later on, this optimal cut is critical to link the two phases of the column generation, preventing many potential columns to be generated in the second phase.

6.3.3. A Lexicographic Objective for Pricing Subproblems In general, sparse columns are more likely to enter the basis in the master problem (M). As a result, the B&P algorithm uses a lexicographic objective in the pricing subproblem. First, it minimizes the (pessimistic or standard) reduced cost. Then it maximizes sparsity by minimizing $1^T w^s$ subject to the constraint that the reduced cost must be equal to the optimal objective value of the first stage.

6.4. The Final Branch and Price Implementation

6.4.1. Column Generation The column generation starts with an initial basis built from the optimal solutions of each subproblems under the objective function of $c^T w^s$. It then proceeds with two phases of column generation, first using the pessimistic reduced cost and then switching to the standard one.

The second phase terminates when the optimality gap becomes lower than the predetermined tolerance, e.g., 0.1%. The lower bound is based on Lagrangian relaxation. Given a pair $\bar{w}$ and $(\bar{y}, \bar{\sigma})$ of optimal primal and dual solutions for (M), the Lagrangian relaxation is given by

$$L(\bar{w}, \bar{y}, \bar{\sigma}) = c^T \bar{w} + \sum_{s \in \mathcal{S}} \mathcal{O}_s(\bar{y}, \bar{\sigma})$$

where $\mathcal{O}_s(\bar{y}, \bar{\sigma})$ is the optimal solution of the pricing problem for scenario s under dual variables $(\bar{y}, \bar{\sigma})$. The first phase uses the same technique for termination, although the resulting formula is no longer guaranteed to be a lower bound. Once the gap between the upper bound and the "approximate" lower bound is smaller than the tolerance, the column generation process moves to the second phase.

The column generation also avoids generating dominated columns. Assume that $[w_1^s = 1, w_2^s = 1]$ is a feasible solution of (P_s) and the corresponding column has been added to the master problem (M). Then, there is no need to consider a solution $[w_1^s = 1, w_2^s = 1, w_3^s = 1]$. The column generation adds the constraint of $w_1^s + w_2^s \leq 1$ to (P_s) when such a dominated solution is produced and does not include it in the master problem.

6.4.2. The Branch and Bound After convergence of the column generation to $LP_{\widetilde{P}}$, the branch and bound algorithm solves the restricted master problem (M) with the integral condition $w \in \{0, 1\}^m$ to obtain a strong primal bound. In general, this incumbent solution is of very high quality and the average optimality gap is 0.19%. Therefore, the branch and price algorithm uses a depth-first branch and bound. Moreover, at each branching node, it selects the variable that minimizes the optimality gap.

7. Description of the Data Sets

This section describes the distribution test systems. The data set is available from `https://github.com/lanl-ansi/micot/` in the `application_data/lpnorm` directory. Details of the data format are available from `https://github.com/lanl-ansi/micot/wiki/Resilient-Design-Executable`.

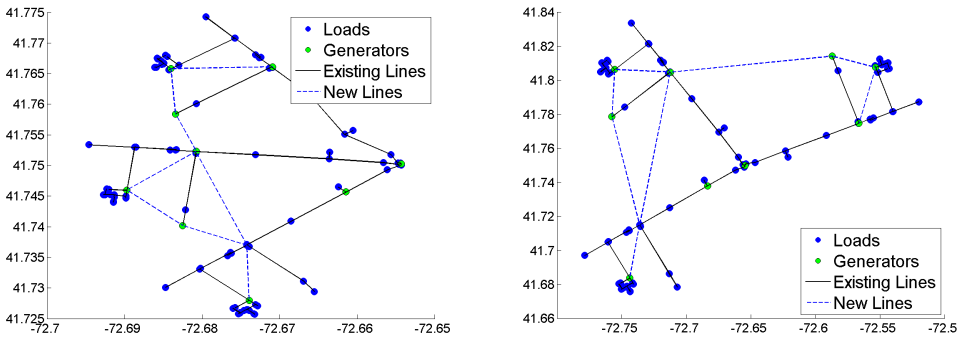

(a) Urban (b) Rural

Figure 5 **The urban and rural distribution systems which contain three copies of the IEEE 34 system to mimic situations where there are three normally independent distribution circuits that support each other during extreme events. These test cases include 109 nodes, 118 generators, 204 loads, and 148 edges.**

The first two sets, the *Rural* and *Urban* systems, is from Yamangil et al. (2015). They are based on the IEEE 34 bus system (Kersting 1991) (see Figure 5) and replicate the 34-bus distribution feeder three times. All three feeders are connected to a single transmission bus and candidate new lines were added to the network to allow back-feeds. In the rural model, the distribution feeder was geolocated to model feeders with long distances between nodes. Similarly, the urban network was geolocated to model compact feeders typical of urban environments. Geolocation of these networks has the net effect of adjusting the lengths of the power lines and their associated impedance values. Spreading the network out also increases the hardening and new line costs. As a result, the rural system is expected to favor solutions with distributed generation and the urban system solutions with new lines and switches (in addition to hardening lines). The fixed cost of installing a new distributed generator is set at \$500k. The cost of a distributed generator is set at \$1,500k per MW based on the 2025 projections from U.S. Energy Information Administration (2014). The cost of installing new switches for 3-phase lines is set between 10k and 50k (Bialek 2014). The cost of new underground 3-phase lines is set at about \$500k per mile and the cost of new underground single phase lines is set at about \$100k per mile. The hardening cost is set at roughly \$50k and \$10k per mile for multi-phase and single-phase lines (State of Virginia Corporation Commission 2005). The third network, NETWORK123, is based on the 123-node network of Kersting (1991). This network is unaltered except for adding new line candidates and labeling large loads as critical.

The communication network $\widetilde{G}$ is built to conform to G. Let $G' = (N', E')$ be the duplicate of G. For each generator $l \in \mathcal{U}$, its duplicate $i(l)$ represents its control point. Consider

$\mathcal{E}'_t \subseteq E'$, the duplicate of $\mathcal{E}_t$. To represent the control point for a switch, $e \in \mathcal{E}'_t$ is divided in the middle and a new vertex v_e is added to represent the control point for the switch. In other words, the edge $e = (e_h, e_t) \in \mathcal{E}'_t$ is replaced by a new vertex v_e and two new edges $e_1 = (e_h, v_e), e_2 = (v_e, e_t)$. The test cases assume that the damage, installation, and hardening of a line in G are also incurred for the corresponding line in $\widetilde{G}$. These assumptions can be easily generalized without changing the nature of the model.

The experimental evaluation considers 100 scenarios per damage intensity for all three networks and the damage intensities are taken in the set {1%, 2%, 3%, 4%, 5%, 10%, 15%, 20%, 25%, 30%, 35%, 40%, 45%, 50%, 55%, 60%, 65%, 70%, 75%, 80%, 85%, 90%, 95%, 100%}. The scenario generation procedure is based on damage caused by ice storms. The intensity tends to be homogeneous on the scale of distribution systems (Sa 2002). Ice storm intensity is modeled as a per-mile damage probability, i.e. the probability at least one pole fails in a one mile segment of power line. Each line is segmented into 1-mile segments and a scenario is generated by randomly failing each segment with the specified probability. This probability is normalized for any line segment shorter than 1 mile. A line is "damaged" if any segment fails.

8. Case Study

This section analyzes the behavior of the optimization model on a variety of test cases. In particular, it studies how the topology of the distribution grid and the dispersion level of its communication network affect the optimal design. For each network described in Section 7, this section analyzes the optimal design under different settings of damage probability, the resiliency level, and the number of communication centers. The default value of η_c and η_t are 98% and 50% respectively, the default number of communication centers is 4, and the phase variation parameter β is set to 15% for E_V and ∞ otherwise. Unless specified otherwise, the comparisons are based on these default values.

8.1. Impact of grid topology

Let n_h, n_x, n_t, and n_u be the number of hardened lines, new lines, new switches, and new generators in the optimal design. Figure 6 reports these values for various damage levels and the three networks. The red line indicates the optimal upgrade costs, and the counts of the upgrade options are represented as a bar. The results show that hardening lines is the major component of each optimal design and that its share increases with the disaster

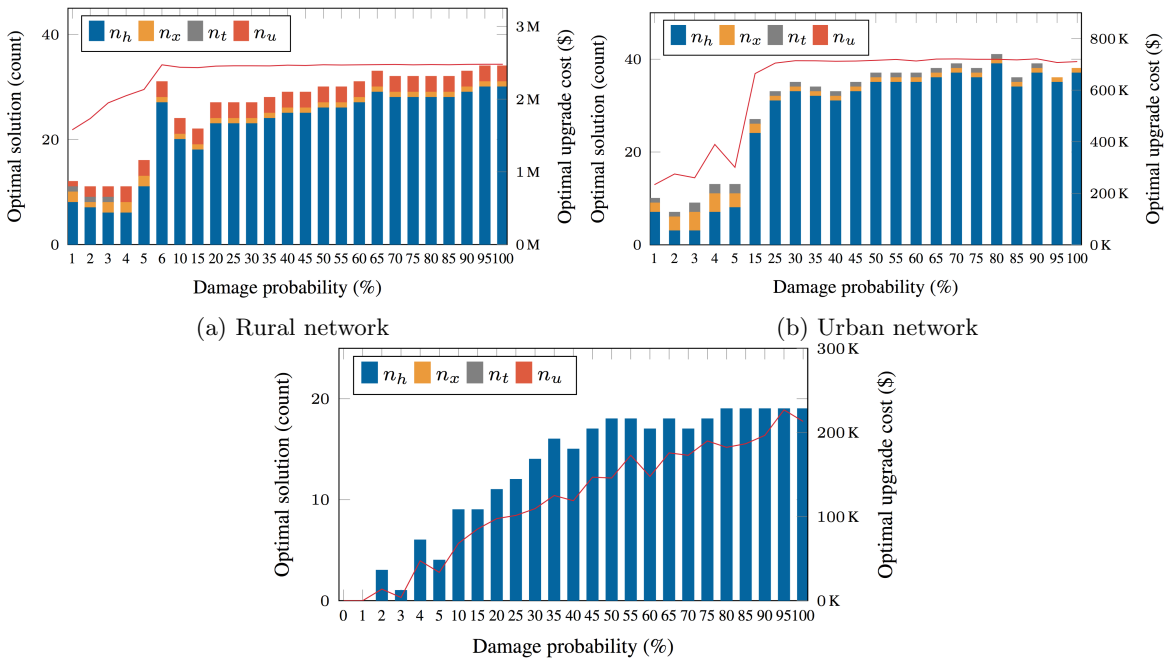

(a) Rural network (b) Urban network

(c) Network123

Figure 6 **Statistics on the Optimal Grid Designs.**

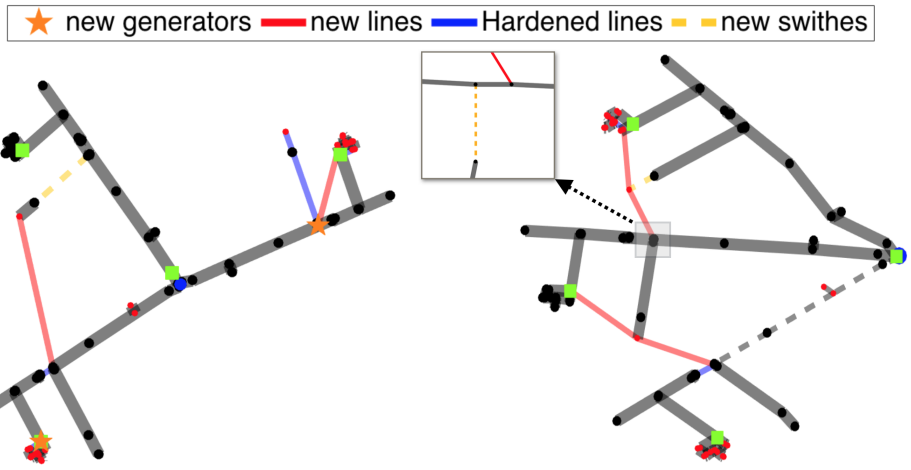

(a) Rural network (b) Urban network

Figure 7 **Optimal Designs of the Rural and Urban Networks (3% damage level).**

intensity. The results also show that DGs are used in significant numbers in the rural network, while new lines and switches complement hardening in the urban model. This was expected given the length of the lines in these two networks. The third network only needs line hardenings.

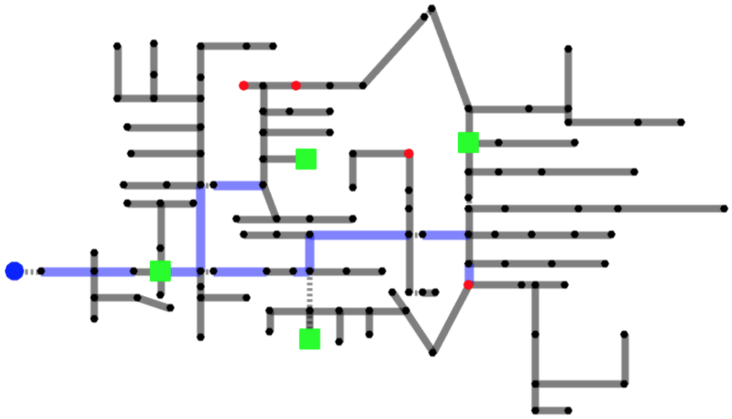

Figure 8 Optimal Design of Network NETWORK123 **(20% damage level).**

8.2. Impact of the Communication Network

First note that ignoring the communication network is equivalent to assuming that every bus has its own communication center. In the following, $\widetilde{G}(k)$ denotes a communication network with k centers and $\widetilde{G}(\infty)$ the case where each bus has a center.

Figure 9 and Table 3 report the impact of the communication system: They report optimal objective values and solution statistics under various numbers of communication centers. Fewer communication centers lead to significant cost increases in the rural network, but have limited effect on the urban network and NETWORK123. In the rural network, resiliency comes from forming microgrids with DGs, which require their own communication centers. When these are not available, optimal designs harden existing lines and build new lines and switches, which are more costly as substantiated in Table 3.

Figure 10 illustrates the resulting designs on the rural network for scenarios with a damage level of 3%. The top row depicts some of the scenarios and shows the affected lines. The bottom row depicts the optimal designs for various configurations of the communication network. For $\widetilde{G}(\infty)$, the optimal design features three new DGs in the west-, north-, and east-end of the network to meet the critical loads of each region. These regions are then islanded under various scenarios. For $\widetilde{G}(4)$, the optimal design installs a new line linking critical loads in the north side to the west side of the network, instead of using DG in the north side. This stems from Scenario 100 where a DG in the bus with critical loads cannot be operated since it has no communication center. For $\widetilde{G}(1)$, scenario 1 prevents the operation of an east-end DG and scenario 100 the operation of a west-end DG. Hence, the optimal design only considers hardening and new lines and switches. On the other hand,

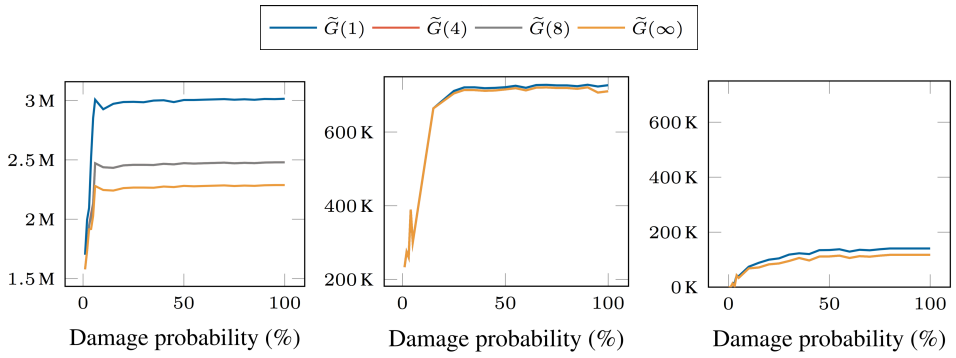

(a) Rural network (b) Urban network (c) Network123

Figure 9 Cost Analysis For the Number of Communication Centers

Table 3 Impact of the Communication Network on Optimal Grid Designs.

	Comm. Network	Obj.	n_h	n_x	n_t	n_u
Rural, 3% damage	$\widetilde{G}(1)$	2095.74	12	3	1	0
	$\widetilde{G}(4)$	1948.09	6	2	1	2
	$\widetilde{G}(8)$	1948.09	6	2	1	2
	$\widetilde{G}(\infty)$	1914.99	5	1	0	3

the urban network and NETWORK123 achieve resiliency by increasing grid connectivity for all communication networks.

9. Load Flow Analysis of the Linearization of the ORDPDC

This section analyzes the accuracy of the linearization explained in Section 4. To simulate the actual load flow of the solution obtained by the linearized ORDPDC, we use the OpenDSS software, a comprehensive electrical power system simulation tool for distribution systems. The experiments consider a random set of 108 instances (approximately 10% of total instances) by setting $\eta_t = 0.5$ and 0.8, and the damage level to 5%, 25%, 45%, 65%, 85%, 100% for the three networks $\widetilde{G}(0)$, $\widetilde{G}(1)$, and $\widetilde{G}(4)$. Each instance has approximately 100 scenarios, which means that the results report the load flow analysis for about 10,800 scenarios.

In our initial experiments, OpenDSS reported that some solutions did not satisfy power flow physics. After analyzing these results, we found a single cause for these infeasibilities– zero flow on lines. In some situations, instead of using switches to remove flow from a line, the solutions based on the linearized model allowed zero flow on a line by letting both end-buses of the line have the same voltage magnitude. In practice, this effect is highly undesirable since it can reverse flows and allow flow from single phase buses to three phase

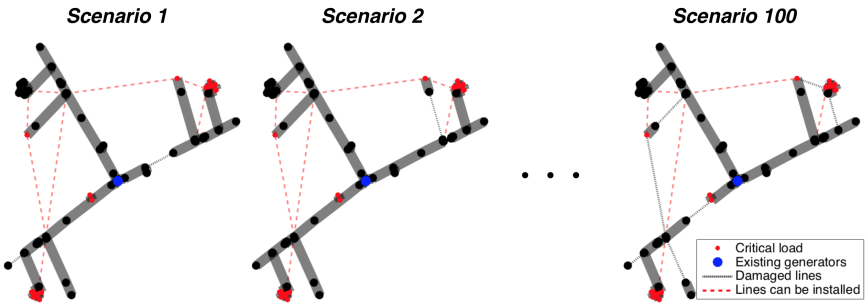

(a) damage scenarios

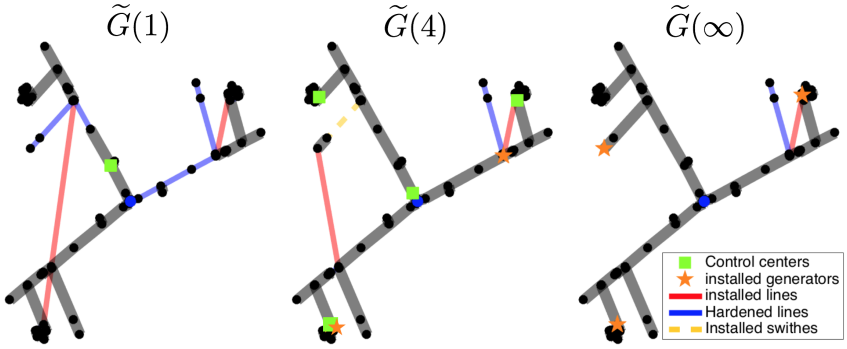

(b) Optimal grid design

Figure 10 **Optimal Designs of the Rural Network under 3% Damage and Various Communication Network Configurations.**

buses. In such cases, even small voltage variation can result in significant voltage drops. Hence, we prevent these situations by adding the following set of constraints:

$$\sum_{e\in P}(x_e - \tau_e) \leq |P| - u_l,\ \forall P \in \mathcal{P}_l,\ l \in \mathcal{U}^n$$

$$\sum_{e'\in P}(x_{e'} - \tau_{e'}) \leq |P| - x_e,\ \forall P \in \mathcal{P}_e,\ e \in \mathcal{E}_x^n$$

where $\mathcal{P}_l$ and $\mathcal{P}_e$ denotes the set of paths that start from bus l with an edge e that has an increasing number of phases (e.g., a line from single phase bus to three phase bus), respectively. These constraints force a switch to be added along such a path, hence preventing the undesirable situation.

Once these constraints were added, the OpenDSS software reported that optimal solutions of the linearized ORDPDC for all 10,800 cases were feasible for the three phase AC power flow physics and satisfy all load and bound constraints.

10. Performance Analysis of the Branch and Price Algorithm

This section studies the performance of the B&P algorithm. All computations were implemented with the C++/Gurobi 6.5.2 interface and OpenMPI. They use a Haswell architec-

ture compute node configured with 24 cores (two twelve-core 2.5 GHz Intel Xeon E5-2680v3 processors) and 128 GB RAM.

10.1. Computational Performance

We compare the computational performance of the B&P algorithm with that of the SD and SBD algorithms in this section. In the implementation of the SD algorithm, we do not update the dual vector, i.e., $\lambda = 0$ for all iterations, as done in the original paper. For all instances, the SD algorithm exhibits a slow convergence rate and could not solve any of them within the wall time limit of 4 hours. That is because the ORDPDC does not satisfy the condition under which the SD algorithm is guaranteed to perform effectively. Indeed, the probability that a solution to a scenario becomes a global solution is very small since quite different scenarios have the same probability in the ORDPDC. Moreover, since there are many combinations of binary variables with similar objective values in the ORDPDC, cutting off already explored solutions improves the lower bound only by a small amount, which leads to a very slow convergence rate.

Figure 11a reports the computation time of the B&P and SBD algorithms for all the instances described in Section 7, where the reference line (in red) serves to delineate when an algorithm is faster than the other. Their statistics are displayed in Figure 11b. In average, the B&P algorithm is faster than the SBD algorithm by a factor of 3.25. These figures also indicate that the SBD algorithm has a high degree of performance variance. This comes from the nature of the scenario set $\mathcal{S}$. If S contains a dominating scenario and the scenario has low index in $\mathcal{S}$, then the SBD algorithm solves the problem quickly. Otherwise, the SBD may need a large number of iterations and the MIP model keeps growing in size with each iteration. For 2 out of 1120 instances, the SBD algorithm times out (wallclock time limit of 4 hours). On the other hand, the B&P algorithm is stable across all instances. The B&P algorithm also has the additional benefit that it produces improving feasible solutions continuously. In contrast, the SBD algorithm only produces a feasible solution at optimality. Finally, the B&P algorithm appears more stable numerically than the SBD algorithm. For 5 out of 1120 instances, the B&P algorithm yields a better optimal solution than the SBD algorithm as shown in Table 4. Each such solution was validated for feasibility.

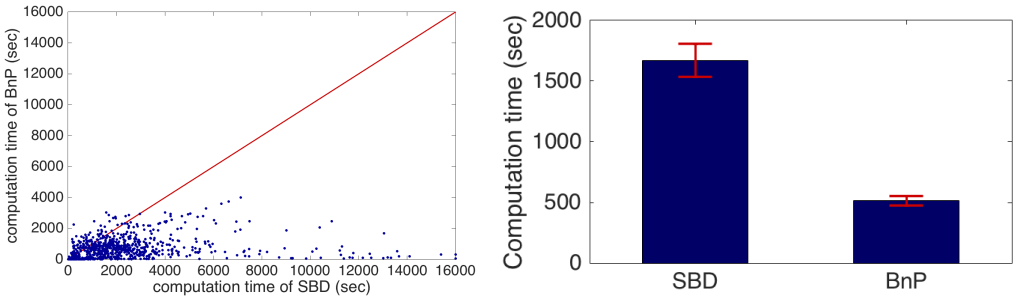

(a) Computation Times

(b) Average Computation Times and 95% Confidence Intervals

Figure 11 Comparison of Computation Times: SBD versus B&P.

Table 4 Numerical Stability of the B&P Algorithm.

Instance	Opt. obj.val		
	SBD	B&P	Gap
Rural, 30% damage, $\eta_t = 0.5$, $\widetilde{G}(4)$	2458.49	2453.79	-0.19 %
Rural, 30% damage, $\eta_t = 0.6$, $\widetilde{G}(4)$	2458.49	2453.79	-0.19 %
Rural, 30% damage, $\eta_t = 0.7$, $\widetilde{G}(4)$	2524.68	2519.98	-0.19 %
Rural, 30% damage, $\eta_t = 0.8$, $\widetilde{G}(4)$	2572.31	2567.60	-0.19 %
Network123, 55% damage, $\eta_t = 0.8$, $\widetilde{G}(8)$	232.48	227.27	-2.24 %

Table 5 Branching Tree Statistics.

Avg. # of branching nodes	Avg. opt. gap at the root node
1.8	0.19 %

10.2. Solution Quality at the Root Node.

The problem reformulation produces a strong lower bound and the majority of the instances are proven optimal at the root node. Table 5 summarizes the average number of branching nodes and the average optimality gap at the root node.

10.3. Benefits of the Accelerating Schemes

To highlight its design choices, the B&P algorithm is compared to a column generation with dual stabilization (Du Merle et al. 1999). In addition, the benefit of each of the accelerating schemes is investigated independently by running the B&P algorithm without the considered extension. We sample 90 instances by setting $\eta_t = 0.5$ and 0.8, and the damage level to 5%, 30%, 65%, 85%, 100% for the three networks $\widetilde{G}(0)$, $\widetilde{G}(1)$, and $\widetilde{G}(4)$. Dual stabilization prevents dual variables from fluctuating too much, which is often the case in column generation. It tries to confine dual variables in a box that contains the current best estimate of the optimal dual solution and penalizes solutions that deviate

Table 6 Comparison to a Column Generation with Dual Stabilization.

	Avg. computation time (sec)	Avg. number of iterations
B&P$_B$	12857.97†	3122.57†
B&P$_S$	11563.44†	1514.58†
B&P	488.03	96.12

from the box. See, for instance, Du Merle et al. (1999), Lübbecke and Desrosiers (2005) for details about stabilized column generation. Our implementation updates the box whenever the Lagrangian lower bound is updated.

Table 6 summarizes the computational performance of the stabilized column generation in comparison with the B&P algorithm. B&P$_B$ denotes the branch-and-price algorithm with the basic scheme only (Section 6.2) and B&P$_S$ stands for the branch and price algorithm with dual stabilization. The symbol † is used to denote that the algorithm reaches the wallclock time limit for some instances. For more than one third of the sampled instances, B&P$_B$ and B&P$_S$ exceed the wallclock time limit. For instances where both algorithms terminate within the time limit, B&P$_S$ is faster than B&P$_B$ by a factor of around 4. Although the dual stabilization does improve the computation time of the basic algorithm, it is still not adequate to solve the ORDPDC practically. The B&P algorithm, on the other hand, shortens computation times by a factor of 26.35.

The next results investigate the performance gain of each accelerating scheme by removing them one at a time from the B&P algorithm. Table 7 describes the computational performance and Figure 12 illustrates the impact of each accelerating schemes on the convergence rate of the rural network under 6% damage level. In the table and figure, R denotes the revised reduced cost, C the optimality cut, O the lexicographic objective pricing problem, B&P$_{\setminus k}$ the B&P algorithm without scheme k, with $k \in \{R, C, O\}$, and CG$_{\setminus k}$ the column generation of B&P without scheme k.

The results in Table 7 indicate that all the accelerating schemes contribute to the computational performance of the B&P algorithm. Figure 12a illustrates the key role of the optimality cut. Without this cut, the second stage of the column generation which uses the traditional pricing objective does not take advantage of the columns generated in the first stage and its lower bound drastically drops. Figure 12b compares the convergence behavior of CG and CG$_{\setminus R}$, showing that CG reaches the optimal objective value faster than CG$_{\setminus R}$. Figure 12c highlights the impact of the lexicographic objective function and shows that it significantly contributes to the fast convergence of the algorithm.

Table 7 Benefits of the Accelerating Schemes.

	Avg. computation time (sec)	Avg. number of iterations
B&P	488.03	96.12
B&P$_{\setminus R}$	844.24	96.39
B&P$_{\setminus C}$	2589.55†	215.94†
B&P$_{\setminus O}$	2979.84†	544.65†

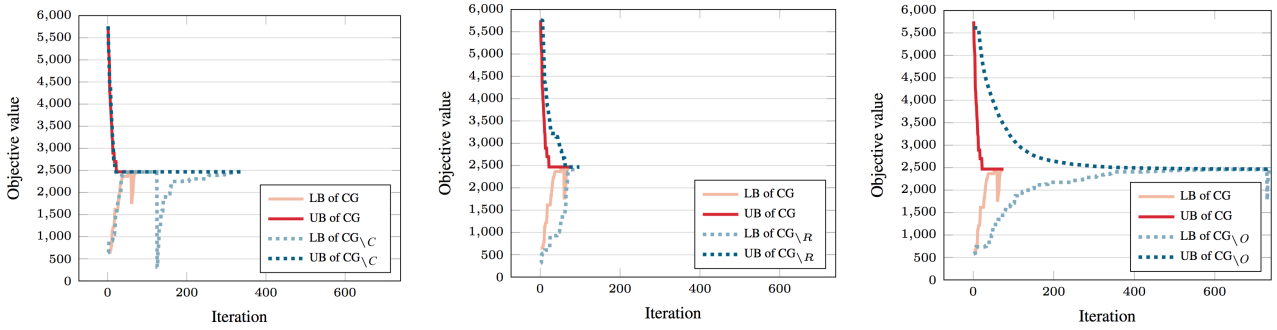

(a) Optimality cut (b) Revised reduced cost (c) lexicographic objective function

Figure 12 Comparison of Convergence Rates (rural network, 6% level of damage).

11. Conclusions

This paper proposed an expansion planning model to improve the resiliency of distribution systems facing natural disasters. The planning model considers the hardening of existing lines and the addition of new lines, switches, and distributed generators that would allow a subpart of the system to operate as a microgrid. The expansion model uses a 3-phase model of the distribution system. In addition, it also considers damages to the communication system which may prevent generators and switches to be controlled remotely. The input of the expansion model contains a set of damage scenarios, each of which specifying how the disaster affects the distribution system.

The paper proposed a branch and price algorithm for this model where the pricing subproblem generates new expansions for each damage scenario. The branch and price uses a number of acceleration schemes to address significant degeneracy in the model. They include a new pricing objective, an optimality cut, and a multi-objective function to encourage sparsity in the generated expansions. The resulting branch and price algorithm significantly improves the performance of scenario-based and scenario decomposition algorithms and a branch and price with a stabilized column generation. The case studies show that optimal solutions strongly depend on the grid topology and the sophistication of the

communication network. In particular, the results highlight the importance of distributed generation for rural networks, which necessitates a resilient communication system.

The acceleration techniques presented in this paper are not limited to the electricity distribution grid planning problem; They can be used on problems with similar structure, i.e, two-stage stochastic problems with feasibility recourse.

Future work will be devoted to applying and scaling these techniques to instances with thousands of components.

Acknowledgements

The work was funded by the DOE-OE Smart Grid R&D Program in the Office of Electricity in the US Department of Energy through the Grid Modernization Laboratory Consortium project, *LPNORM*. It was carried out under the auspices of the NNSA of the U.S. DOE at LANL under Contract No. DE-AC52-06NA25396. It was also partly supported by National Science Foundation grant NSF-1638331.

References

Ahmed S (2013) A scenario decomposition algorithm for 0–1 stochastic programs. *Operations Research Letters* 41(6):565–569.

Amor HMB, Desrosiers J, Frangioni A (2009) On the choice of explicit stabilizing terms in column generation. *Discrete Applied Mathematics* 157(6):1167–1184.

Barnes A, Nagarajan H, Yamangil E, Bent R, Backhaus S (2017) Tools for improving resilience of electric distribution systems with networked microgrids. *CoRR* abs/1705.08229, URL `http://arxiv.org/abs/1705.08229`.

Bialek T (2014) Private Communications, San Diego Gas and Electric.

Carvalho P, Ferreira L, Da Silva AC (2005) A decomposition approach to optimal remote controlled switch allocation in distribution systems. *IEEE Transactions on Power Delivery* 20(2):1031–1036.

Chen C, Wang J, Qiu F, Zhao D (2016) Resilient distribution system by microgrids formation after natural disasters. *IEEE Transactions on smart grid* 7(2):958–966.

Ding T, Lin Y, Li G, Bie Z (2017) A new model for resilient distribution systems by microgrids formation. *IEEE Transactions on Power Systems* .

Du Merle O, Villeneuve D, Desrosiers J, Hansen P (1999) Stabilized column generation. *Discrete Mathematics* 194(1-3):229–237.

Executive Office of the President (2013) Economic Benefits of Increasing Electric Grid Resilience to Weather Outages. Technical report.

Falahati B, Fu Y, Wu L (2012) Reliability assessment of smart grid considering direct cyber-power interdependencies. *IEEE Transactions on Smart Grid* 3(3):1515–1524.

Gan L, Low SH (2014) Convex relaxations and linear approximation for optimal power flow in multiphase radial networks. *Power Systems Computation Conference (PSCC), 2014*, 1–9 (IEEE).

Gao H, Chen Y, Xu Y, Liu CC (2016) Resilience-Oriented Critical Load Restoration Using Microgrids in Distribution Systems. *IEEE Trans. on Smart Grid* PP(99):1–1, ISSN 1949-3053, URL `http://dx.doi.org/10.1109/TSG.2016.2550625`.

Gholami A, Aminifar F, Shahidehpour M (2016) Front lines against the darkness: Enhancing the resilience of the electricity grid through microgrid facilities. *IEEE Electrification Magazine* 4(1):18–24.

Kersting W (1991) Radial distribution test feeders. *IEEE Transactions on Power Systems* 6(3):975–985, ISSN 08858950, URL `http://dx.doi.org/10.1109/59.119237`.

Lasseter R, Akhil A, Marnay C, Stephens J, Dagle J, Guttromson R, Meliopoulous A, Yinger R, Eto J (2002) The certs microgrid concept. *White paper for Transmission Reliability Program, Office of Power Technologies, US Department of Energy* 2(3):30.

Li Z, Shahidehpour M, Aminifar F, Alabdulwahab A, Al-Turki Y (2017) Networked microgrids for enhancing the power system resilience. *Proceedings of the IEEE* 105(7):1289–1310, ISSN 0018-9219, URL `http://dx.doi.org/10.1109/JPROC.2017.2685558`.

Lübbecke M, Desrosiers J (2005) Selected topics in column generation. *Operations Research* 53(6):1007–1023.

Martins L, Girao-Silva R, Jorge L, Gomes A, Musumeci F, Rak J (2017) Interdependence between power grids and communication networks: A resilience perspective. *DRCN 2017-Design of Reliable Communication Networks; 13th International Conference; Proceedings of*, 1–9 (VDE).

McCormick GP (1976) Computability of global solutions to factorable nonconvex programs: Part i—convex underestimating problems. *Mathematical programming* 10(1):147–175.

Oukil A, Amor HB, Desrosiers J, El Gueddari H (2007) Stabilized column generation for highly degenerate multiple-depot vehicle scheduling problems. *Computers & Operations Research* 34(3):817–834.

Panteli M, Trakas DN, Mancarella P, Hatziargyriou ND (2017) Power systems resilience assessment: Hardening and smart operational enhancement strategies. *Proceedings of the IEEE* 105(7):1202–1213, ISSN 0018-9219, URL `http://dx.doi.org/10.1109/JPROC.2017.2691357`.

Parhizi S, Lotfi H, Khodaei A, Bahramirad S (2015) State of the art in research on microgrids: A review. *IEEE Access* 3:890–925.

Resende F, Gil N, Lopes J (2011) Service restoration on distribution systems using multi-microgrids. *International Transactions on Electrical Energy Systems* 21(2):1327–1342.

Sa Y (2002) *Reliability Analysis of Electric Distribution Lines*. Ph.D. thesis, McGill University.

Schrijver A (1998) *Theory of linear and integer programming* (John Wiley & Sons).

State of Virginia Corporation Commission (2005) Placement of Utility Distribution Lines Underground. Technical Report House Document 30, Governor and the General Assembly of Virginia, Richmond, VA.

US Energy Information Administration (2014) Annual Energy Outlook 2014. Technical report, URL `http://dx.doi.org/DOE/EIA-0383(2014)`.

Wang Y, Chen C, Wang J, Baldick R (2016a) Research on resilience of power systems under natural disasters—a review. *IEEE Transactions on Power Systems* 31(2):1604–1613.

Wang Z, Chen B, Wang J, Chen C (2016b) Networked microgrids for self-healing power systems. *IEEE Transactions on smart grid* 7(1):310–319.

Xu Y, Liu CC, Schneider KP, Ton DT (2016) Placement of remote-controlled switches to enhance distribution system restoration capability. *IEEE Transactions on Power Systems* 31(2):1139–1150.

Yamangil E, Bent R, Backhaus S (2015) Resilient upgrade of electrical distribution grids. *AAAI*, 1233–1240.

Yuan C, Illindala MS, Khalsa AS (2017) Modified viterbi algorithm based distribution system restoration strategy for grid resiliency. *IEEE Transactions on Power Delivery* 32(1):310–319.

Yuan W, Wang J, Qiu F, Chen C, Kang C, Zeng B (2016) Robust optimization-based resilient distribution network planning against natural disasters. *IEEE Transactions on Smart Grid* 7(6):2817–2826.